Water Resources Research

RESEARCH ARTICLE
10.1029/2019WR026303

Spatiotemporal Variability in Transport and Reactive Processes Across a First- to Fifth-Order Fluvial Network

Kaylyn S. Gootman[1,2], Ricardo González-Pinzón[3], Julia L. A. Knapp[4], Vanessa Garayburu-Caruso[3,5], and Jaye E. Cable[1,2]

[1]Environment, Ecology, and Energy Program, University of North Carolina at Chapel Hill, Chapel Hill, NC, USA, [2]Department of Marine Sciences, University of North Carolina at Chapel Hill, Chapel Hill, NC, USA, [3]Department of Civil, Construction and Environmental Engineering, University of New Mexico, Albuquerque, NM, USA, [4]Department of Environmental Systems Science, ETH Zurich, Zurich, Switzerland, [5]Pacific Northwest National Laboratory, U.S. Department of Energy, Richland, WA, USA

Key Points:
- Reactive tracer tests revealed reaction-limited conditions along a first- to fifth-order fluvial network during contrasting flow regimes
- Processing rate coefficients and Damköhler numbers decreased along the continuum
- Results support modeling expectations of decreasing hyporheic contributions along fluvial networks

Supporting Information:
- Supporting Information S1

Correspondence to:
K. S. Gootman and R. González-Pinzón,
kaylyn.gootman@mail.wvu.edu;
gonzaric@unm.edu

Citation:
Gootman, K. S., González-Pinzón, R., Knapp, J. L. A., Garayburu-Caruso, V., & Cable, J. E. (2020). Spatiotemporal variability in transport and reactive processes across a first- to fifth-order fluvial network. *Water Resources Research*, *56*, e2019WR026303. https://doi.org/10.1029/2019WR026303

Received 10 SEP 2019
Accepted 31 MAR 2020
Accepted article online 6 APR 2020

Abstract Fluvial networks integrate, transform, and transport constituents from terrestrial and aquatic ecosystems. To date, most research on water quality dynamics has focused on process understanding at individual streams, and, as a result, there is a lack of studies analyzing how physical and biogeochemical drivers scale across fluvial networks. We performed tracer tests in five stream orders of the Jemez River continuum in New Mexico, USA, to quantify reach-scale hyporheic exchange during two different seasonal periods to address the following: How do hyporheic zone contributions to overall riverine processing change with space and time? And does the spatiotemporal variability of hyporheic exchange scale across fluvial networks? Combining conservative (i.e., bromide) and reactive (i.e., resazurin) tracer analyses with solute transport modeling, we found a dominance of reaction-limited transport conditions and a decrease of the contributions of hyporheic processing across stream orders and flow regimes. Our field-based findings suggest that achieving knowledge transferability of hyporheic processing within fluvial networks may be possible, especially when process variability is sampled across multiple stream orders and flow regimes. Therefore, we propose a shift in our traditional approach to investigating scaling patterns in transport processes, which currently relies on the interpretation of studies conducted in multiple sites (mainly in headwater streams) that are located in different fluvial networks, to a more cohesive, network-centered investigation of processes using the same or readily comparable methods.

1. Introduction

Streams and rivers transport resources essential for terrestrial and aquatic life (Krause et al., 2011; Woessner, 2000; Wohl, 2015). In these fluvial systems, biogeochemical constituents are transformed in riparian, benthic, and hyporheic zones. These zones of rapid turnover play an important role in small- to large-scale riverine ecological functioning due to the transfer of mass and energy between two contrasting but complementary environments, i.e., surface and ground waters (Boano et al., 2014; Fischer et al., 2005; Hester et al., 2017; Magliozzi et al., 2018; Nowinski et al., 2011; Orghidan, 1959). The dynamic and spatially varying groundwater and surface water mixing zone provides an ideal physical habitat for microbial communities, which benefit from increased resources and contact times under a range of redox conditions (Brunke & Gonser, 1997; Gooseff, 2010; Woessner, 2000).

Research interest in the hyporheic zone, and its functional significance, has steadily grown in recent years (Ward, 2016; Ward et al., 2019). However, most studies focus on hyporheic exchange in small, easily construed headwater streams rather than in large rivers (Tank et al., 2008; Hall et al., 2013; González-Pinzón et al., 2015a; Ward et al., 2019). Over the past three decades, more than 80% of hyporheic zone studies have been conducted in low-order (i.e., first, second, and third) streams, as defined by Strahler (1952) (Figure 1). Low-order streams offer research advantages to studying hyporheic exchange because they are small, abundant, tractable, more easily constrained, and more accessible than their larger-order counterparts (Ensign & Doyle, 2006; Gooseff et al., 2013; Tank et al., 2008; Ward, 2016). Low-order streams also make up a large proportion of reach lengths throughout many fluvial networks, highly influencing

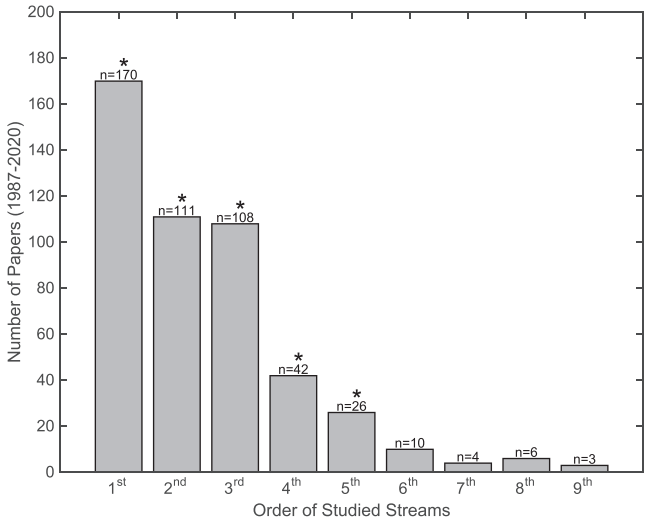

Figure 1. Number of hydrologic studies published using data from first- to ninth-order streams between 1987 and 2020. The journal articles were found using a targeted search query using Elsevier's Scopus search engine on 18 March 2020. Search terms included "transient storage" or "hyporheic" in addition to "stream order" from article titles, abstracts, and key words. Asterisks (*) indicate the stream orders that were targeted in this study.

regional water quality and ecological functioning (Alexander et al., 2007; Freeman et al., 2007; Gomez-Velez & Harvey, 2014).

In addition to making up a larger proportion of catchment reach lengths, low-order streams are thought to have greater influence over hyporheic zone processing than their high-order counterparts throughout various fluvial networks. For example, Gomez-Velez et al. (2015) found that vertical hyporheic excursions into the streambed generally decreased with increasing stream order in the Mississippi River network, meaning that watershed hyporheic contributions to overall riverine processing decreased with increasing stream order over large spatial scales. Additionally, shallower stream depths, typically found in low-order streams, maintain closer contact between surface water and reactive bed sediments and may encourage higher streambed reaction rates (Harvey & Gooseff, 2015). The expectation of decreasing hyporheic zone processing relative to total riverine processing with increasing stream order is in line with hydrologic and geomorphic assumptions underlying upscaling approaches due to greater water volumes and thus less relative exchange, finer streambed sediments resulting in a lower hydraulic conductivity, and greater river depth in higher-order streams (Harvey & Gooseff, 2015; Wondzell, 2011). Thus, the general expectation is that as stream volume increases (i.e., discharge), the relative contribution of hyporheic exchange processing decreases. However, this scaling expectation has rarely been tested in the same fluvial network across different stream orders, as studying hyporheic exchange in larger rivers involves many experimental challenges. As river size and flow rates increase, it can become impractical or difficult to apply methods traditionally used in small stream orders like tracer testing, due to reduced stream accessibility associated with geographic and anthropogenic complexity, increased tracer costs, and increased distances required to have comparable residence times (González-Pinzón et al., 2015a; Tank et al., 2008; Xie & Zhang, 2010).

The limited data available from the few field studies investigating reach-scale processes in larger rivers suggest that they may play an important role in nutrient spiraling and that the fluxes between aquatic and terrestrial environments in those systems may be equally significant and comparable to their smaller-order counterparts (Ensign & Doyle, 2006; González-Pinzón et al., 2015b; Hall et al., 2013; Tank et al., 2008). Therefore, this field-based evidence seems to contradict the expectation that small-order streams have greater biogeochemical potential than larger-order streams (Gomez-Velez & Harvey, 2014; Wondzell, 2011) and highlights the need to investigate hyporheic zone contributions across individual fluvial networks to support within- and across-network understanding of hyporheic zone processing (Boano et al., 2014; Pinay et al., 2015; Wondzell, 2011). Ultimately, the uncertainty in how hyporheic exchange contributes to overall riverine processing across a range of stream orders and flow regimes hinders our ability to predict catchment-wide water quality outcomes and their influence on water resource management (Graf, 2001; Groffman et al., 2009; Harvey & Gooseff, 2015; Magliozzi et al., 2018; McClain et al., 2003; Stonedahl et al., 2013; Stream Solute Workshop, 1990; Tank et al., 2008; Ward, 2016).

In this study, we explored hyporheic exchange dynamics from spatial and temporal perspectives using *in situ* measurements from within the same fluvial network to address two questions: (1) How do hyporheic zone contributions to riverine processing change with space and time? And (2) does the spatiotemporal variability of hyporheic exchange scale across fluvial networks? We present and discuss the results of eight reactive tracer tests using the resazurin-resorufin (Raz-Rru) system (Haggerty et al., 2008; Knapp et al., 2018). These tests were done in five different stream orders along the Jemez River, New Mexico (Figure 2a), during two different flow regimes (i.e., summer baseflow and spring higher flow). The Raz-Rru system was chosen for this study because the irreversible transformation of Raz to Rru provides an *in situ* estimation of hyporheic zone processing as a fraction of riverine processing through an estimation of metabolic activity (Dallan et al., 2020; Haggerty et al., 2008; González-Pinzón et al., 2012, 2014, 2016; González-Pinzón et al., 2015b; Knapp & Cirpka, 2018). While not all the parameters describing reactive transport across the Jemez River network varied consistently with stream order or discharge, we found a trend toward more

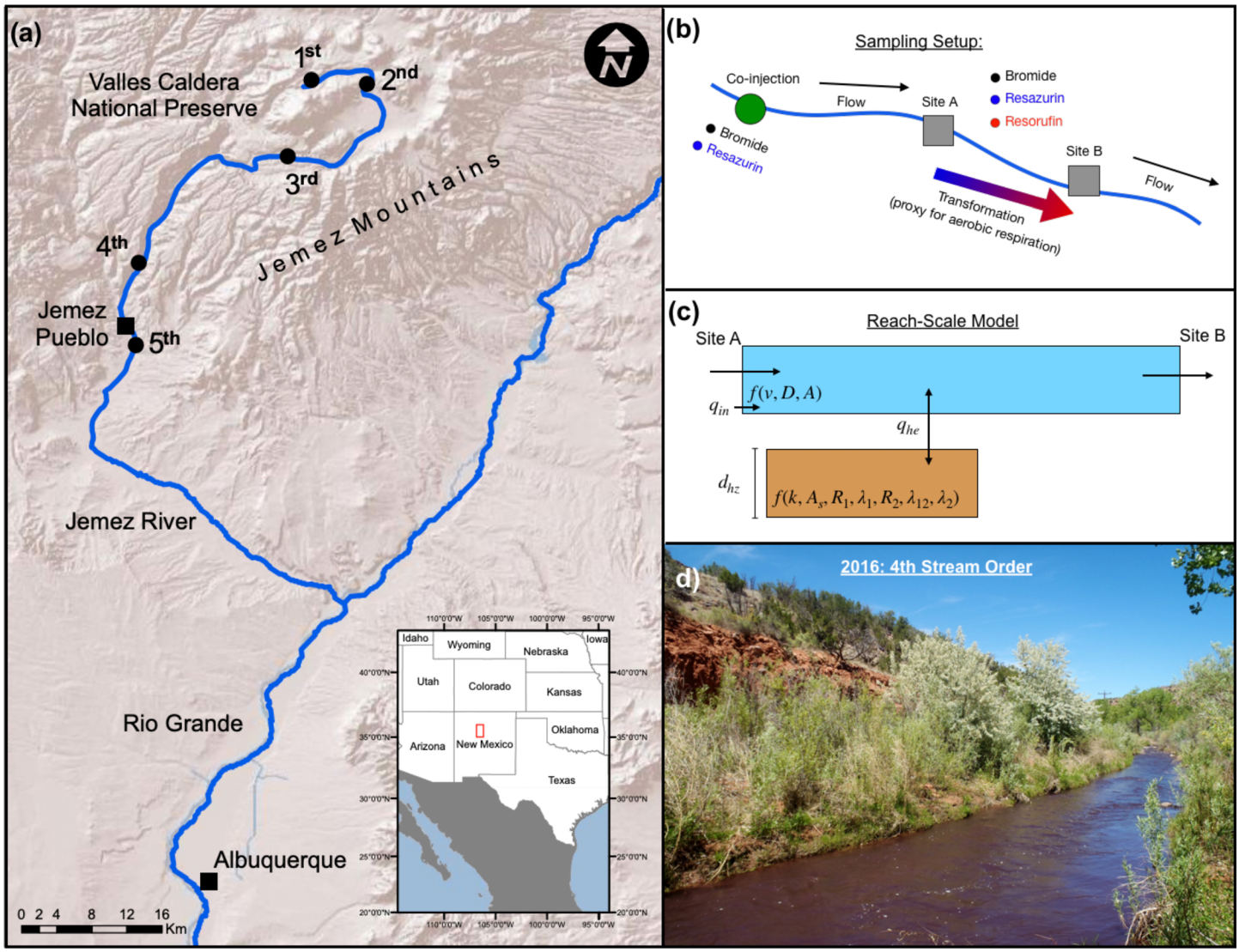

Figure 2. A map of the Jemez River shows (a) our study reach locations highlighted along the river with black circles; (b) diagram detailing the field sampling setup for each stream order reach where bromide and resazurin were injected and analyzed with samples from two downstream sampling stations, Site A and Site B; (c) the transient storage model conceptualization used for the reach-scale analysis, with two downstream sampling stations Site A and Site B, considering in-stream (blue box) and hyporheic zone (brown box) parameters; (d) photo taken during a tracer injection at the fourth-order stream reach in 2016.

reaction-limited conditions with increasing discharge across all stream orders, as Damköhler numbers consistently decreased along the fluvial network in response to decreasing processing rate coefficients.

2. Materials and Methods

2.1. Description of Field Sites

We completed reactive tracer tests in five different stream orders of the Jemez River watershed during contrasting flow regimes of the same time period (June 2015, i.e., summer baseflow, and May/June 2016, higher spring flow conditions). The Jemez River is located in northern New Mexico (Figure 2a) and drains an area of 2,678 km^2 before becoming a tributary to the Rio Grande (USGS National Water Information System, 2018). The upper portion of the watershed is forested with a mix of subalpine balds, aspen groves, mixed conifer, spruce, ponderosa, and riparian zone grasslands (Coop & Givnish, 2007; Small & McConnell, 2008). This region is characterized by a semiarid, continental climate with temperatures ranging from −5.4 °C in January to 15 °C in July (New Mexico Climate Center, 2018). The lower portion of the Jemez

Table 1
Study Reach Sampling Date, Stream Order, Average Stream Discharge ($m^3 s^{-1}$), Stream Depth (m), Width (m), Channel Area (m^2), Estimated Mixing Length (km), Study Reach Length (km), Porosity (%), Mean Water Temperature (°C), and Elevation Above Sea Level (km) for the 2015, i.e., Lower-Flow, and 2016, i.e., Higher-Flow, Sampling Campaigns

Sampling date	Stream order	Discharge ($m^3 s^{-1}$)	Stream depth (m)	Stream width (m)	Channel area (m^2)	Mixing length (km)	Reach length (km)	Porosity (%)	Mean water temperature (°C)	Elevation (km)
2015	*Baseflow (dry season)*					Inj-A	A-B			
27 Jun	1	0.014	0.20	1.82	0.36	0.65	0.57	59	18.78	2.75
26 Jun	2	0.020	0.16	2.23	0.42	1.03	0.54	47	18.50	2.64
25 Jun	3	0.090	0.16	3.00	0.47	0.76	2.63	27	19.56	2.46
24 Jun	4	0.160	0.23	4.15	1.20	1.24	2.75	35	24.38	1.81
23 Jun	5	0.180	0.22	7.65	1.71	2.98	1.47	27	25.17	1.72
2016	*Receding (wet season)*									
3 Jun	1	0.001	0.05	0.35	0.02	0.41	0.01	59	16.56	2.82
16 May	2	0.110	0.38	1.09	0.41	1.46	0.63	47	21.00	2.68
20 May	3	0.500	0.23	4.80	1.11	1.77	2.80	27	14.20	2.45
21 May	4	0.790	0.32	3.00	1.58	2.23	3.77	35	19.18	1.81

River watershed contains shrub/grassland vegetation and has an arid climate with temperatures ranging from 1.0 °C in January to 26 °C in July (Homer et al., 2015; New Mexico Climate Center, 2018).

Local precipitation averages 639 mm yr^{-1} at higher elevations and 210 mm yr^{-1} at lower elevations including rain and snowfall (New Mexico Climate Center, 2018). Annual stream high flows occur during the peak spring snowmelt period, and annual stream low flows occur during the summer season (USGS, 2018). The Jemez River is known for hydrothermal inputs which influence riverine chemical equilibrium through dynamic water-rock interaction processes such as dissolution and weathering (McIntosh et al., 2017; White et al., 1992). The portion of the river that runs through the Valles Caldera National Preserve is particularly well studied and known for contributing to the salinization of the Jemez River (McGibbon et al., 2018). Historical river basin geology consists of igneous and metamorphic complexes, along with sedimentary and volcanic deposits (Cibils et al., 2008; Coop & Givnish, 2007; Craig, 1992; Smith et al., 1970). Streambed substrates sampled during our experiments along the Jemez River continuum consisted of poorly sorted small boulders, gravel, and sand and included a range of fine particle fractions.

The tracer experiments took place between 23 June and 27 June 2015 and between 16 May and 4 June 2016 (Table 1 and Figure 2a). Reach length was measured as the distance between each pair of sampling stations of the respective stream order using Google Earth imagery (Google Earth, Google, Mountainview, California, USA). Discharge was gaged during the tracer tests with an acoustic Doppler velocimeter (SonTek/YSI FlowTracker ADV; SonTek, San Diego, California, USA) using the midsection method (Terzi, 1981). Discharge was quantified from a series of observation verticals and measured at representative locations ($n = 3$) of each study reach, including at the injection location, Site A, and Site B (Figure 2b). The discharge values reported in Table 1 reflect the average discharge for each reach before the tracer tests were conducted.

In 2015, study reach lengths and discharge varied from 0.57 to 2.75 km and 0.014 to 0.180 $m^3 s^{-1}$, respectively (Table 1). In 2016, study reach lengths and measured discharge varied from 0.01 to 3.77 km and >0.001 to 0.790 $m^3 s^{-1}$, respectively (Table 1). It should be noted that the subreaches between 2015 and 2016 were not identical due to differences in stream discharge, which required the use of different mixing lengths between the injection site and the most upstream sampling location. The differences in discharge between the two sampling years represent seasonal differences in flow between dry, baseflow conditions in the summer months and wet, snowmelt conditions in the spring season. *In situ* surface water temperature was monitored with multiparameter water quality sondes (EXO2 Sonde, YSI Incorporated, Yellow Springs, Ohio, USA) and ranged from 18.50 to 25.17 °C in 2015 and from 14.20 to 21.00 °C in 2016.

Table 2
Injected Tracer Co-Injection (g), Initial Travel Time (hr), Reach Travel Time (hr), Simulated Surface Water Bromide Mass Recoveries (hr), Simulated Surface Water Resazurin Mass Recoveries (%), and the Resazurin to Bromide Recovery Ratio (–) for the 2015, i.e., Baseflow, and 2016, i.e., Higher Flow, Sampling Campaigns

Sampling date	Stream order	Mass injection NaBr (g)	Mass injection Raz (g)	Reach travel time (hr)	Reach Br^- recovery (%)	Reach Raz recovery (%)	Raz/Br^- recovery ratio
2015				A to B	A to B	A to B	
27-Jun	1	200	10	1.55	36	13	0.36
26-Jun	2	50	10	1.85	55	50	0.91
25-Jun	3	900	50	3.90	65	55	0.85
24-Jun	4	900	60	2.39	63	63	1.00
23-Jun	5	600	60	2.37	65	62	0.95
2016							
3-Jun	1			n.a.			
16-May	2	152	28	0.77	92	92	1.00
20-May	3	500	90	1.84	88	85	0.97
21-May	4	1,400	133	1.77	84	84	1.00
6-Jun	5			n.a.			

Note. The results from the first-order stream in 2016 were excluded from the analysis because the model fit did not yield acceptable results. Additionally, high discharges in 2016 did not allow us to complete the experiments in the fifth-order stream.

Streambed sediment grab samples ($n = 15$) of approximately 300 g were collected from the thalweg of each stream order near the injection location, Site A, and Site B, to quantify porosity for the first- through fifth-order streams during the 2016 sampling campaign (Table 1) (Vomocil, 1965; Wroblicky et al., 1998). Porosity was determined from measured sediment particle and dry bulk densities (Fetter, 2001). We assumed the 2016 porosity measurements were representative of our studied stream orders in both sampling periods. Porosity was generally higher at the lower stream order sites where the streambed sediments were dominated by sand size particles, as was expected from the bedload fining associated with higher stream orders (Ren & Packman, 2007), due to the streambed mix of gravel and sand size particles.

2.2. Experimental Setup and Field Sampling

We coinjected bromide (Br^-) and resazurin (Raz) via instantaneous tracer injections (Table 2). Raz is a redox-sensitive phenoxazine dye that can be used as a "smart" tracer to estimate microbiological activity associated with stream water-sediment interactions (González-Pinzón et al., 2012; Haggerty et al., 2008; Knapp et al., 2018). In the presence of mildly reducing conditions, Raz undergoes an irreversible reduction to its daughter product resorufin, Rru, and experimental work with microbial communities has shown that (1) the transformation of Raz to Rru is proportional to oxygen consumption (González-Pinzón et al., 2012) and (2) the mass balance of Raz and Rru closes over time scales relevant for field experiments (Dallan et al., 2020). Therefore, the transformation from Raz to Rru has been used as a proxy for *in situ* aerobic metabolism and water-sediment interactions in the last decade (Argerich et al., 2011; González-Pinzón et al., 2014, 2016; González-Pinzón et al., 2015b; Knapp & Cirpka, 2018; see review by Knapp et al., 2018).

In our experiments, injected tracer masses were adjusted to stream discharge to guarantee sufficiently high tracer concentration across sites. We sampled the breakthrough curves (BTCs) of Br^-, Raz, and Rru at two stations (i.e., Site A and Site B) downstream of the injection site (Figure 2b). Site A was always the first downstream sampling station, and Site B was always downstream of Site A. Downstream distances between the injection location and the first sampling station, Site A, varied based on estimated tracer mixing lengths. BTCs were sampled for periods ranging from 4 to 10 hr after injection. These sampling periods were deemed sufficient to capture the Raz to Rru reaction time scale (<6 hr) (Dallan et al., 2020; González-Pinzón et al., 2012). Surface water grab samples were collected from the thalweg at each of the sampling stations at intervals ranging from every 1 to 30 min throughout our tracer BTCs using 60 ml plastic syringes and were filtered through 0.45 μm pore size Whatman Nylon filters (25 mm diameter). Filtered samples were placed inside a dark cooler with ice immediately after sampling and later refrigerated at 4 °C until they were analyzed in the laboratory, always within 48 hr after sampling.

2.3. Laboratory Analysis

Each water sample was aliquoted (1.0 ml) and buffered to pH 8.5 before fluorescence was read (Haggerty et al., 2008, 2009). All water samples were analyzed for Raz and Rru fluorescence signals with a spectrofluorometer (Varian Cary Eclipse; Santa Clara, California) at excitation/emission wavelengths of 602/632 nm for Raz and 571/584 nm for Rru. Fluorescence readings were converted to concentrations with the help of calibration standards and using the MATLAB code available in Knapp et al. (2018). The limit of quantification (LOQ) for Raz was 1.01×10^{-1} mol L^{-1} and 1.67×10^{-3} mol L^{-1} for Rru. The remainder of each grab sample was frozen at −20 °C and stored in the dark until they could be thawed and analyzed for Br^- with ion chromatography using a Dionex ICS-1000 Ion Chromatograph with AS23/AG23 analytical and guard columns, and a 1,000 μl injection loop with a Br^- analytical limit of detection (LOD) of 1.67×10^{-3} mol m^{-3} (Thermo Fisher Scientific Inc.; Sunnyvale, California). Ion chromatograph standards were prepared using a multielement solution from SCP Science (Champlain, NY) and were analyzed at the beginning and end of the run. Initial calibration verification (ICV) standard solution was analyzed after calibration standards to verify the quality of the calibration curve, and continuing calibration verification (CCV) standard solution was run every 20 samples, with deionized water blanks before and after the CCV to account for potential calibration drifts. ICV and CCV acceptable criteria was ±10% of the expected value.

2.4. Transient Storage Modeling

The model used in this work describes the one-dimensional in-stream, reach-scale transport of the tracer compounds undergoing exchange with the hyporheic zone during the transit downstream with uniform and time-invariant coefficients (Figure 2c; Knapp et al., 2017). The model applied here is similar to the one made available as a MATLAB script in Knapp et al. (2018) with the addition of a dilution term. It considers the hyporheic zone as a single, well-mixed, transient storage zone that undergoes linear exchange with the main channel, accounts for the compound specific behavior of Raz and Rru in the hyporheic zone, and estimates surface water dilution due to groundwater inflow between sampling stations (Lemke et al., 2014; Runkel, 1998). Although the exponential transit time distribution resulting from the linear exchange between the two modeled compartments may not be an ideal representation of hyporheic zone residence times (Haggerty, 2002; Gooseff et al., 2005), we used it in an effort to obtain a parsimonious model.

Model results yielded effective bulk estimates of streambed reactivity but did not provide information about the spatial distribution of these processes. The coupled governing equations for Br^- ($i = 0$), Raz ($i = 1$), and the reaction product Rru ($i = 2$) are

$$\frac{\partial c_i}{\partial t} + \frac{A_s}{A} R_i \frac{\partial c_{hz,i}}{\partial t} + v \frac{\partial_{C_i}}{\partial x} - D \frac{\partial^2 c_i}{\partial x^2} = \frac{A_s}{A} r_{hz,i} + q_{in}\left(c_{in,i} - c_i\right) \tag{1}$$

$$R_i \frac{\partial c_{i,hz}}{\partial t} = k\left(c_i - c_{hz,i}\right) + r_{hz,i} \tag{2}$$

subject to the following initial and boundary conditions of an instantaneous tracer injection:

$$c_i(x,\, t = 0) = c_{hz,i}(x,\, t = 0) = 0 \forall x \tag{3}$$

$$\left(v c_i - D \frac{\partial c_i}{\partial x}\right)\Big|_{x=0} = \frac{M_i}{A} \delta(t) \tag{4}$$

$$\lim_{x \to \infty} c_i(x,\, t) = 0 \forall t \tag{5}$$

in which c_i (mol·m^{-3}) denotes the compound concentration in the main channel; $c_{hz,i}$ (mol·m^{-3}) represents the compound concentration in the transient storage zone; the in-stream advective velocity is given by v (m s^{-1}); D (m^2 s^{-1}) represents the dispersion coefficient; A_s/A, (–) represents the ratio of the cross-sectional area of the storage zone A_s (m^2) to that of the stream A (m^2); the reaction rate is given by $r_{hz,i}$ (mol m^{-3} s^{-1}); q_{in} represents the dilution factor (s^{-1}) for gaining reaches; $c_{in,i}$ denotes the concentration of the groundwater inflow, where $c_{in,i} = 0$ for all tracers; the first-order mass transfer rate coefficient for exchange with the storage zone is given by k (s^{-1}); and M_i (mol) represents the injected tracer mass, except for resorufin where $M_2 = 0$.

The equilibrium sorption coefficient of compound i in the hyporheic zone is represented by R_i (–), assuming linear sorption at local equilibrium. Since bromide is a conservative tracer that neither undergoes sorption or transformation, we set

$$R_0 = 1 \text{ and } r_{hz,0} = 0$$

whereas both resazurin and resorufin may sorb in the streambed ($R_1 \geq 1; R_2 \geq 1$). Raz and Rru streambed chemical transformation were assumed to follow first-order kinetics (González-Pinzón & Haggerty, 2013), resulting in the following reaction rates:

$$r_{hz,1} = -\lambda_1 c_{hz,1} \tag{6}$$

$$r_{hz,2} = \lambda_{12} c_{hz,1} - \lambda_2 c_{hz,2} \tag{7}$$

in which λ_1 (s^{-1}) is the total Raz transformation rate coefficient; λ_{12} (s^{-1}) is the Raz-to-Rru transformation rate coefficient, with $\lambda_{12} \leq \lambda_1$ since the transformation of Raz to Rru cannot exceed the total transformation of Raz; and λ_2 (s^{-1}) is the Rru transformation rate coefficient. The previous equations were solved in the Laplace domain and back-transformed numerically (Hollenbeck, 1998; Knapp et al., 2017).

Details on the model calibration procedure are presented in the supporting information (Text S1). Briefly, model parameter estimation was completed using the Differential Evolution Adaptive Metropolis (DREAM [ZS]) algorithm (Vrugt et al., 2009). Parameters for Br^- and Raz were jointly estimated in a first step of 100,000 model generations. Rru-specific parameters were estimated separately from an additional 100,000 generations, while all parameters related to Br^- and Raz were sampled from their previously determined distributions. Model convergence was assessed using Gelman and Rubin (1992) $\widehat{R}$ statistics, and the agreement between measured and simulated BTCs was quantified through the calculation of the residual sum of squares, ($nRSS$) (–), normalized by the squared theoretical peak tracer concentrations of each tracer BTC of the respective tracer at the given location. The median of the best 1,000 model simulations were used to assess the agreement between our final model fits and a subset of possible curve fits.

2.4.1. Tracer Recoveries, Transport, and Reaction Metrics

Tracer recoveries in Table 2 were quantified using an analysis of the zeroth temporal moments of the simulated BTCs (Harvey & Gorelick, 1995). The zeroth temporal moments at Site A, $\mu_0(x_A)$ (mol s m^{-3}), and Site B, $\mu_0(x_B)$ (mol s m^{-3}), over time t (s) for Br^- ($i = 0$) and Raz ($i = 1$) were defined as

$$\mu_{0,i}(x_A) = \int_0^\infty c_i(x_A, t)\mathrm{d}t \tag{8}$$

$$\mu_{0,i}(x_B) = \int_0^\infty c_i(x_B, t)\mathrm{d}t. \tag{9}$$

Mean reach travel times, τ (hr), were calculated from the normalized first temporal moments (Harvey & Gorelick, 1995; Lemke et al., 2013) of the simulated conservative tracer at Site A, $m_{1,0}(x_A)$ (hr), and Site B, $m_1(x_B)$ (hr):

$$m_{1,0}(x_A) = \frac{\int_0^\infty c_0(x_A, t)t\ \mathrm{d}t}{\mu_{0,0}(x_A)} \tag{10}$$

$$m_{1,0}(x_B) = \frac{\int_0^\infty c_0(x_B, t)t\ \mathrm{d}t}{\mu_{0,0}(x_B)} \tag{11}$$

$$\tau = m_{1,0}(x_B) - m_{1,0}(x_A). \tag{12}$$

Tracer mass recovery (Table 2) of compound i along each stream reach was calculated as follows from the simulated BTCs:

$$r_i = \frac{\mu_{0,i}(x_B)}{\mu_{0,i}(x_A)}. \tag{13}$$

For Br^- we expect recovery <1 if discharge increased between A and B due to the dilution of the tracer, whereas the recovery of Raz at Site B was expected to be reduced by both dilution and reaction and consequently $r_1 < r_0$. We thus determined the recovery of Raz relative to Br^- by r_1/r_0.

The reach-scale hyporheic exchange rate coefficient, q_{he} (s^{-1}), represents the volume of water exchanged with the subsurface per time and river volume and was evaluated using parameters from the above transient storage model (Knapp et al., 2017; Liao & Cirpka, 2011):

$$q_{he} = \frac{A_s}{A} k. \tag{14}$$

The apparent depth of the hyporheic zone, d_{hz} (cm), was calculated from the relative size of the transient storage zone and measured field parameters:

$$d_{hz} = \frac{A_s}{A} A_{meas} \frac{1}{w_{hz}\theta}. \tag{15}$$

where A_{meas}(cm^2) was the measured cross-sectional area of the stream, w_{hz}(cm) was the width of the hyporheic zone, approximated by the measured channel width, and porosity, θ (–). Additionally, the mean hyporheic zone residence times for the study reach, τ_{hz} (s), were determined from the inverse of the fitted transient storage model first-order exchange rate coefficient, k (s^{-1}):

$$\tau_{hz} = \frac{1}{k}. \tag{16}$$

Damköhler numbers quantify the time scale of the residence and reaction along hyporheic flow paths (Ensign & Doyle, 2005; Harvey et al., 2013; Harvey & Fuller, 1998; Oldham et al., 2013), providing insight into the factors limiting reaction progress in the hyporheic zone (Harvey et al., 2005; Ocampo et al., 2006). Reach-scale Damköhler numbers, *Da* (–), were calculated for each reach using the following equation:

$$Da = \tau_{hz}\lambda_1. \tag{17}$$

Values of *Da* near 1 indicate a relative balance between transport and reaction time scales, which theoretically result in maximal hyporheic zone reactivity. When *Da* is considerably smaller than 1, processing is reaction limited, and subzones of inactivity are created along hyporheic flow paths. During conditions where *Da* is greater than 1, streambed substrates become transport limited, and inactive hyporheic zone sections contribute to additional storage time but do not support additional reactions (González-Pinzón & Haggerty, 2013; Harvey et al., 2013; Wagner & Harvey, 1997).

We also calculated effective, $\lambda_{eff,hz}$ (s^{-1}), and volume-averaged processing rate coefficients, $\lambda_{\theta,hz}$ (s^{-1}), to quantify how processing changes throughout the Jemez River fluvial network. $\lambda_{eff,hz}$ combines information from mass transfer and reaction rate coefficients to provide information about hyporheic zone-specific processing while accounting for dilution. $\lambda_{\theta,hz}$ scales $\lambda_{eff,hz}$ by the relative size of the hyporheic zone with respect to the main channel. Therefore, both processing terms allow us to assess scaling patterns with stream order and the associated increase in discharge. The following relationships for effective and volume-averaged processing rate coefficients were determined with the following equation modified from González-Pinzón and Haggerty (2013):

$$\lambda_{\theta,hz} = \frac{A_s}{A}\left(\frac{k\lambda_1}{\mathrm{k} + \lambda_1} + q_{in}\right) = \frac{A_s}{A}\lambda_{eff,hz}. \tag{18}$$

3. Results and Discussion

3.1. Model Application and Performance

For each stream order, we obtained 10 unique, best fit transient storage model parameters from the analysis of the 54 surface water BTCs (18 BTCs per tracer compound) sampled along the network (supporting information Table S1). Figure 3 exemplifies the measured and modeled tracer BTCs for the fourth-order stream, and all other sites are shown in the supporting information (Figures S1–S4). Table 2 presents the temporal moments estimated from the simulated BTCs, and Figure 4 shows the resulting parameter estimates along

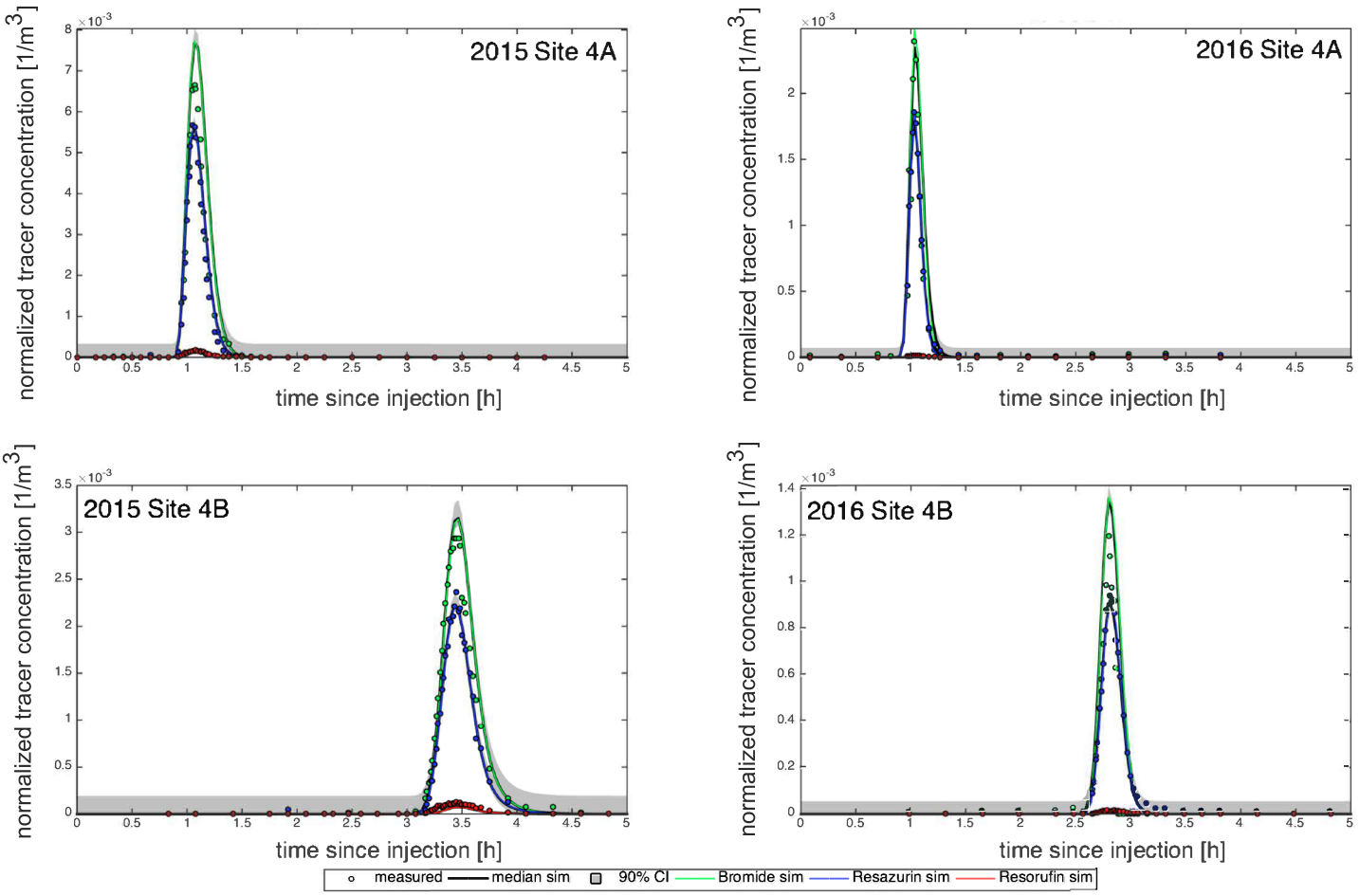

Figure 3. Measured (points), median of the best 1,000 model simulations (black), and best modeled breakthrough curves for bromide (green), resazurin (blue), and resorufin (red), with the 90% confidence interval of the median curve from the last 1,000 model simulations (gray) at the two downstream sampling stations (A: upstream; B: downstream) in the fourth-order stream reach from the 2015 and 2016 sampling campaigns (Site 4). All plotted tracer concentrations were normalized by the number of injected moles to allow for better comparison across BTCs. Measured and simulated BTCs for the other sites can be found in the supporting information (Figures S1–S4).

the fluvial network. The BTC tracer data can be found online with the CUAHSI HydroShare Program (Gootman et al., 2020).

Each of our model parameter estimates resulted in an $\widehat{R}$ statistic (Gelman & Rubin, 1992) that confirmed good model convergence. The quality of the presented simulations, as indicated by the *nRSS* values in supporting information Table S1, shows that our modeling approach provided a robust method for describing in-stream transport and hyporheic exchange processing across the five different stream orders, even with some misfits between measured and simulated data at the BTC peaks. The general agreement between the final BTC simulations and the median simulation of the best 1,000 model generations support the use of our model parameter optimization (Figure 3 and the supporting information Figures S1–S4), as the results typically converged to the best attainable fit to the measured data with the given model results from 100,000 simulations. The downstream Br^- fit at the first stream order in 2016 largely overestimated the Br^- peak likely because either our sampling missed the true peak concentration or there were significant groundwater inputs. Since our data cannot resolve this duality, we did not include those BTCs in any subsequent analyses.

The quality of the model fits was supported by the small parameter uncertainties from the joint fit of Br^- and Raz. Higher parameter uncertainties for the Rru-specific parameters, as indicated by larger $nRSS_{rru}$ values, are likely due to error propagation from the Br^- and Raz joint fit on to the Rru fit and uncertain or correlated

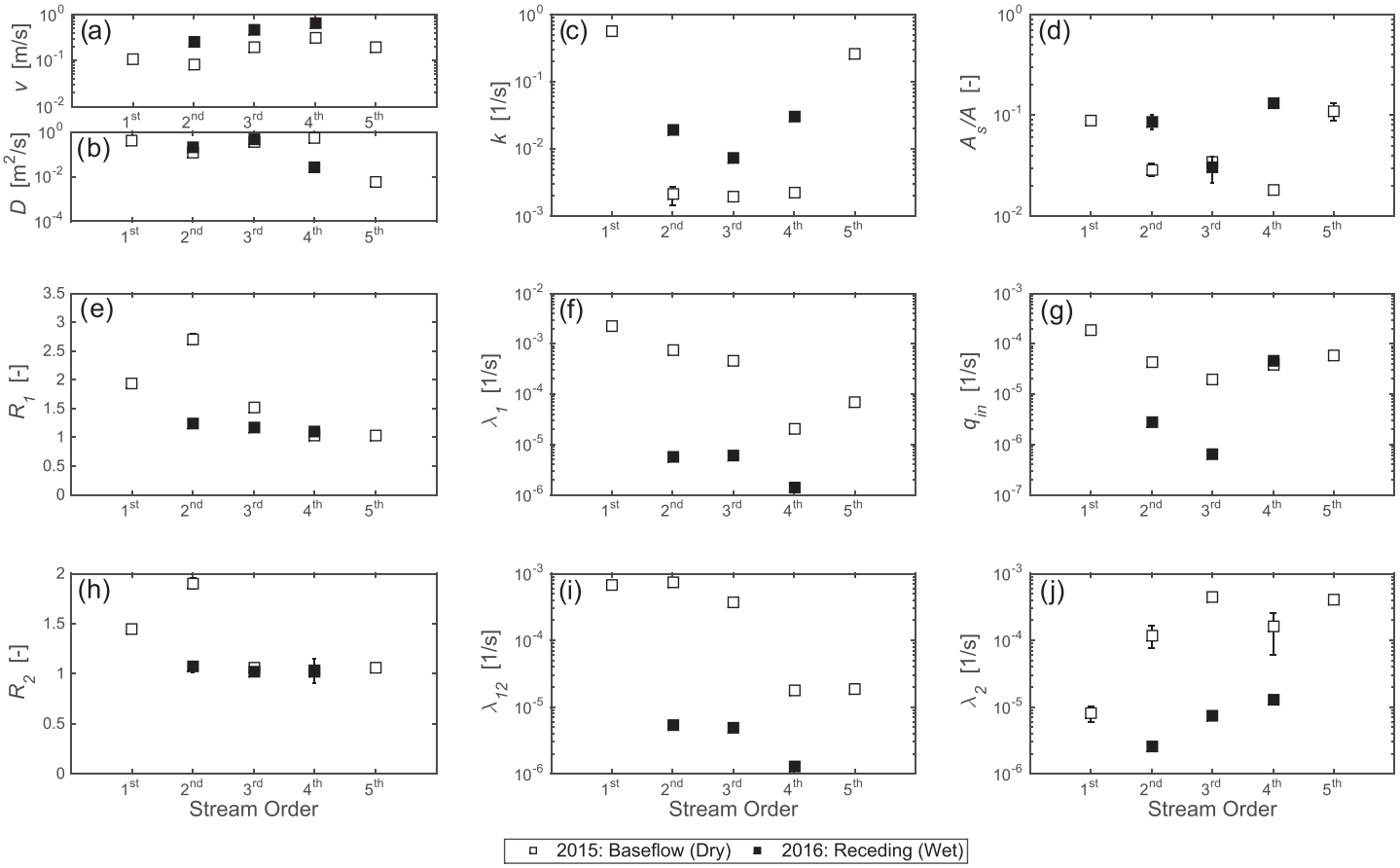

Figure 4. Model parameters ($\pm 1\sigma$) for the 2015, i.e., baseflow, and 2016, i.e., higher flow, sampling campaigns. v (m s^{-1}) is in-stream advective velocity (a); D (m^2 s^{-1}) represents the dispersion coefficient (b); k (s^{-1}) is the mass transfer rate coefficient (c); A_S/A, (–) is the ratio of the cross-sectional area of the storage zone A_s (m^2) to that of the stream A (m^2) (d); R_1 (–) is the retardation factor of resazurin (e); λ_1 (s^{-1}) is the total resazurin transformation rate coefficient (f); q_{in} (s^{-1}) represents the dilution factor (g); R_2 (–) is the retardation factor of resorufin (h); λ_{12} (s^{-1}) is the transformation of resazurin to resorufin rate coefficient; (i) and λ_2 (s^{-1}) is the resorufin transformation rate coefficient (j). The first stream order from 2016 was excluded from these results due to poor model fits of the conservative tracer.

parameters. This additional step amplifies any encountered uncertainties during the second, Rru-related fit. Following Knapp et al. (2017), we therefore chose to interpret hyporheic processes based on the transformation of Raz alone. Rru measurements were used to confirm that the measured Rru BTCs could be simulated with the estimated model parameters.

We additionally analyzed parameter correlations to inform about the reliability of our model parameters. These results are presented in the supporting information (Text S2 and Figures S5–S12) and indicate that our model parameters generally converged on a single value. A sensitivity analysis indicated how the resulting Raz BTCs responded to different parameter values (supporting information Figures S13–19), and revealed that the BTC peaks were typically more sensitive to advective velocity during both flow regimes. BTC tails were more sensitive to dispersion and the mass transfer rate coefficients. Additionally, we found greater uncertainty in the BTC tails, as indicated by the larger confidence intervals along the tails of our BTC plots, due to the lower tracer concentrations in these BTC regions (Payn et al., 2008).

3.2. Parameter Variability Across and Within Stream Orders

For both low and high flow regimes, we found that dispersion, D, the mass transfer rate coefficient, k, the total transformation rate coefficient of Raz, λ_1, and groundwater dilution coefficient, q_{in}, varied up to 3 orders of magnitude across reaches and 2 orders of magnitude within comparable stream reaches (Figure 4 and Table 3). Other parameters such as velocity, the relative size of the storage zone, and the

Table 3
Parameter Variability Across and Within Reaches Shown by the Orders of Magnitude Difference Across All Studied Stream Reaches and Within All Pairs of Studied Stream Reaches

Parameter	Symbol (Unit)	Orders of magnitude difference across all reaches		Orders of magnitude difference within reaches across two seasons (stream order with maximum value, if ≥1)[c]	
		Min[a]	Max[b]	Min	Max
Stream velocity	v (m s^{-1})	<1	1	<1	1 (second)
Dispersion	D (m^2 s^{-1})	<1	2	<1	1 (fourth)
Mass transfer rate coefficient	k (s^{-1})	<1	2	<1	1 (second, fourth)
Relative storage area	A_s/A (−)	<1	1	<1	1 (fourth)
Retardation	R_1 (−)	<1	<1	<1	<1
Reactivity	λ_1 (s^{-1})	<1	3	1 (fourth)	2 (second, third)
Groundwater dilution	q_{in} (s^{-1})	<1	3	<1	2 (third)

Note. The time and space scales for stream behavior are estimated from the greatest differences in parameters.
[a]The term "Min" is the minimum difference in orders of magnitude between all measured stream orders. [b]The term "Max" is the maximum difference in orders of magnitude between all measured stream orders. [c]If difference within a pair of stream orders was greater than or equal to 1 order of magnitude, the stream order was noted in parentheses, thus highlighting where the greatest parameter variability occurred by sampling season.

Raz retardation coefficient varied by ≤1 order of magnitude across all stream reaches. These results suggest that processes specific to reactive transport are affected more strongly by spatial and temporal variability than those specific to conservative transport.

Dispersion, D, and mass transfer rate coefficients, k, displayed greater variability across sites during the drier conditions of 2015, when they varied 2 orders of magnitude compared to 1 order of magnitude in 2016 (Figure 4). Based on our modeling results, for three (second-, third-, and fourth-order streams) of the five stream orders where we had data from both flow regimes, k values increased with flow, while the total transformation rate coefficients of Raz, λ_1, decreased (Figure 4f). These differences may be attributed to how seasonal flow differences influence transient storage.

Dilution coefficients, q_{in}, displayed similar patterns with increasing stream order to λ_1 during both sampling years, with the exception of the fourth stream order in 2016 where q_{in} increased by 2 orders of magnitude from the third-order stream that year (Figure 4g). This indicates that q_{in} decreased with increasing stream order, up until the fourth-order stream. The variability of q_{in} values did not show a systemic pattern as a function of season.

3.3. Hyporheic Exchange Rate Coefficient

The reach-scale hyporheic exchange rate coefficient, q_{he}, varied up to 3 and 2 orders of magnitude across and within reaches, respectively (Table 4). In 2015, the rate of hyporheic exchange decreased from the first to the fourth stream orders before increasing in the fifth-order stream. During this drier sampling period, the fifth-order stream reach had a q_{he} value that was similar to that of the first-order stream. In 2016, q_{he} was highest in the second stream order and did not follow a consistent pattern further downstream. The high variability in both hyporheic exchange rate, as well as the mass transfer rate coefficients, and the absence of a pattern with flow regime or season may indicate the importance of local morphology and stream bed characteristics on hyporheic exchange and processing.

When we normalize q_{he} values by modeled in-stream velocity, v, we can compare them to other studies that also evaluated hyporheic exchange contributions throughout fluvial networks on a per-meter basis (supporting information Table S2). This normalization allows comparisons between our values and those reported in other studies (e.g., Wondzell, 2011), to assess patterns in hyporheic contributions across spatial gradients. Our results generally indicated decreasing hyporheic contributions per meter with increasing stream order, which aligns with other studies (e.g., Boulton et al., 1998; Patil et al., 2013; Ward et al., 2013), with the caveat of the fifth-order stream outlier.

3.4. Hyporheic Zone Depth

The hyporheic zone depth, d_{hz}, varied less than 1 order of magnitude (Table 4). Our values of d_{hz} were within expected ranges compared to other hyporheic zone studies (Harvey et al., 2012; Knapp et al., 2017). The

Table 4
Calculated Hyporheic Exchange Rate Coefficient, $q_{he} \pm 1\,\sigma\,(s^{-1})$, Hyporheic Zone Depth, $d_{hz} \pm 1\,\sigma$ (cm), Residence Time, $\tau_{hz} \pm 1\,\sigma$ (min), Damköhler Number $\pm 1\,\sigma$ (–), Volume-Averaged Processing Rates, $\lambda_{\theta,hz} \pm 1\,\sigma\,(s^{-1})$, and Effective Processing Rates, $\lambda_{eff,hz} \pm 1\,\sigma\,(s^{-1})$ in 2015 (Baseflow) and 2016 (Higher Flow)

Year	Order	q_{he} (s^{-1})	d_{hz} (cm)	τ_{hz} (min)	Da (–)	$\lambda_{\theta,\ hz}$ (s^{-1})	$\lambda_{eff,\ hz}$ (s^{-1})
2015	1	4.9e-2 ± 1.6e-3	3.3 ± 0.1	3.0e-2 ± 9.0e-6	3.9e-3 ± 7.4e-5	2.1e-4 ± 5.3e-2	2.4e-3 ± 6.1e-1
	2	6.1e-5 ± 2.8e-5	1.1 ± 0.2	7.9 ± 2.5	3.6e-1 ± 1.2e-1	1.7e-5 ± 5.0e-5	6.0e-4 ± 1.7e-3
	3	6.5e-5 ± 4.8e-6	2.2 ± 0.1	8.8 ± 0.2	2.4e-1 ± 1.9e-2	1.3e-5 ± 6.8e-5	3.8e-4 ± 2.0e-3
	4	4.0e-5 ± 8.2e-6	1.0 ± 0.1	7.6 ± 0.9	9.1e-3 ± 2.1e-2	1.0e-6 ± 8.5e-6	5.8e-5 ± 4.7e-4
	5	2.9e-2 ± 7.3e-3	9.4 ± 1.9	6.4e-2 ± 3.5e-3	2.6e-4 ± 4.6e-5	1.4e-5 ± 2.6e-4	1.3e-4 ± 2.4e-3
2016	2	1.7e-3 ± 2.3e-3	6.7 ± 1.1	0.9 ± 1.1	3.0e-4 ± 7.8e-4	7.3e-7 ± 5.1e-6	8.4e-6 ± 5.5e-5
	3	5.4e-4 ± 1.0e-4	7.0 ± 0.9	2.3 ± 0.2	8.0e-4 ± 1.2e-4	4.8e-7 ± 7.3e-6	6.6e-6 ± 9.9e-5
	4	3.9e-3 ± 4.0e-4	8.2 ± 0.4	5.6e-1 ± 3.0e-2	4.7e-5 ± 1.9e-4	6.2e-6 ± 1.2e-4	4.7e-5 ± 8.9e-5

Note. Values were quantified using the reach-scale model results, which represent the best fitting simulated breakthrough curves for each stream order.

depth of the hyporheic zone was roughly the same from the first to fourth orders but very different between the two flow regimes, indicating that discharge had a stronger effect than stream order on hyporheic zone extent. The depths were greater during the wetter sampling period than their baseflow counterparts, which is to be expected with greater hydraulic gradients during higher flow periods. Similarly, the greater depth in the fifth-order stream during 2015 baseflow conditions can be attributed to the larger volume of water traveling though this higher-order reach. These results suggest that stream order may only affect hyporheic zone depth as a secondary variable, while stream flow may influence the size of the hyporheic zone and the capacity of a stream section to process reactive solutes directly.

3.5. Hyporheic Zone Residence Time

The hyporheic zone residence time, τ_{hz}, varied 1 and 2 orders of magnitude within and across reaches, respectively (Table 4). The lower limit of our range of τ_{hz} values was smaller than other reach-scale studies (Harvey & Fuller, 1998; Knapp et al., 2017; Knapp & Cirpka, 2017). In 2015, τ_{hz} values were 2 orders of magnitude shorter in first- and fifth-order streams compared to the other sites. In 2016, the second-order stream had a travel time up to 2 orders of magnitude higher than travel time across all reaches (Table 4).

3.6. Hyporheic Zone Processing Rates

The comparison of processing or transformation rate coefficients with stream order and discharge provides insight into how reactive transport scales along fluvial networks. In our study, volume-averaged processing rates coefficients $\lambda_{\theta,hz}$, and effective processing rates, $\lambda_{eff,hz}$, spanned 3 orders of magnitude in 2015, while in 2016 values of $\lambda_{\theta,hz}$ and $\lambda_{eff,hz}$ were within the same order of magnitude. This indicates that greater discharge during spring snowmelt limited processing variability throughout the second-, third-, and fourth-order reaches of the Jemez River (Table 4). Thus, drier conditions resulted in a greater range of solute processing rates in 2015. We found that $\lambda_{\theta,hz}$ and $\lambda_{eff,hz}$ significantly decreased with increasing discharge as evidenced by power law relationships and the corresponding coefficients of determination ($r^2 = 0.44$ and $r^2 = 0.60$, respectively; supporting information Figures S34 and S35 and Table S3). Similarly, we found that the total Raz transformation rate coefficient, λ_1, significantly decreased with increasing discharge ($r^2 = 0.80$; supporting information Figure S25, and Table S3).

3.7. Damköhler Numbers

Damköhler numbers, *Da*, provide a useful way to look at patterns in hyporheic exchange from a nondimensional perspective and have been used to classify riverine processing across different spatial scales (Harvey et al., 2013; Krause et al., 2017; Ocampo et al., 2006; Pinay et al., 2015). In our study, *Da* varied 4 orders of magnitude across reaches and 3 orders of magnitude within reaches (Table 4). For all sites and flow regimes, $Da<1$ indicated the prevalence of reaction-limited conditions, with the second- and third-order streams in 2015 demonstrating near-balanced conditions (Figure 5a). Reaction-limited conditions suggest that if more biomass were present, more processing could occur for the substrates being delivered to bioactive zones (biomass limitation) (Harvey et al., 2013). Alternatively, these conditions may also occur when stoichiometric imbalances result in substrate colimitations, even if plentiful supply and biomass are available (Harvey

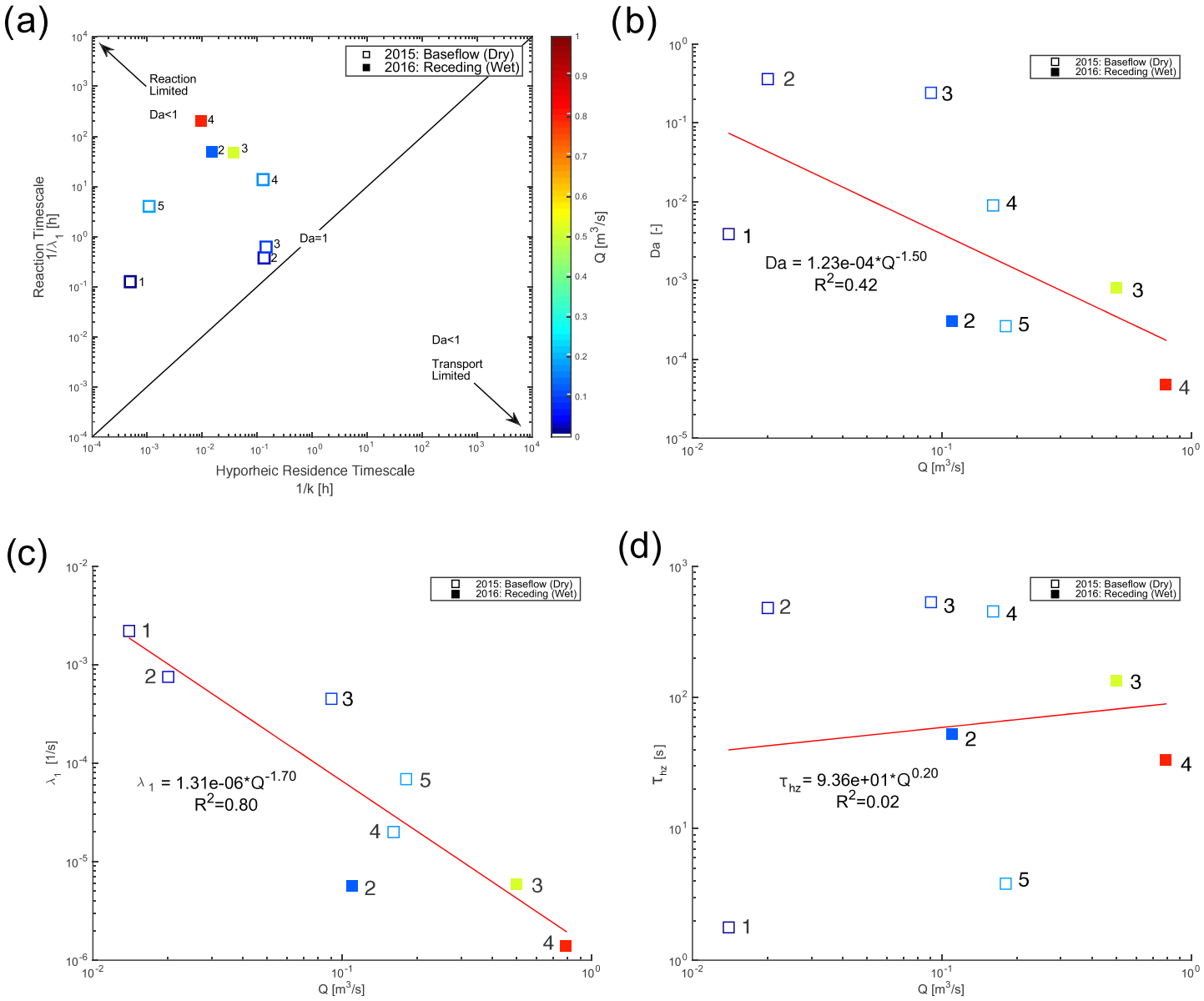

Figure 5. (a) Dimensionless Damköhler scaling of bulk hyporheic zone reactivity. Reaction time scales, λ_1^{-1} (hr), increased during receding conditions, while hyporheic residence time scales, $\tau_{hz} = 1/k$ (hr), varied in response to wetter conditions. Receding conditions created more reaction-limited conditions in the fourth-order stream reach while greatly increasing the magnitude of reaction-limited conditions in remaining order stream reaches. The second- and third-order stream reach time scales moved from near-balanced conditions to reaction-limited conditions due to wetter conditions. Measured discharge, Q ($m^3\ s^{-1}$), is indicated by the color bar scale. Correlation plots for (b) Damköhler number, (c) λ_1, and (d) τ_{hz} versus discharge. Power law relationships between each pair of variables, along with their corresponding coefficients of determination, are shown in panels (b)–(d).

et al., 2005; Ocampo et al., 2006). It is important to note that the uncertainties in *Da* are high due to the additive uncertainties of the hyporheic residence time and the transformation rate coefficient of Raz.

We found decreasing *Da* values with increasing discharge, which suggests that reaction limitations became more important than supply limitations. Our results differ from findings of previous data-guided modeling studies that assumed constant reaction rates, which resulted in increased *Da* with increasing stream flow (e.g., Alexander et al., 2000; Harvey et al., 2019). As such, the variability in our results reflects the heterogeneity in riverine solute processing and provides valuable insights into how spatiotemporal variability influences streambed processing.

To better understand how the drivers of reaction and transport scale across the Jemez River fluvial network, we assessed the relationship between discharge and *Da* as well as its components of reaction and transport, λ_1 and τ_{hz}, using a Spearman rank correlation analysis, which is a test used to assess the relationship between our selected metrics. The strength and direction of the relationship is indicated by ρ, while the significance is determined from a p value. Our Spearman rank correlation analysis revealed a statistically significant decrease of *Da* ($\rho = -0.14$, $p < 0.05$) and λ_1 ($\rho = -0.83$, $p = 0.01$) with increasing discharge and an insignificant correlation between τ_{hz} and discharge ($\rho = -0.14$, $p > 0.1$). Furthermore, we observed that the statistically significant relationships may be described by a power law function (Figures 5b–5d). Taken together, these results suggest an inverse relationship between discharge and transport/reaction metrics, which is mainly driven by the relationship between the reaction rate and discharge. Thus, as discharge and stream order increase, we expect bulk hyporheic activity to decrease. We propose that other fluvial network field studies take a similar paired parametric/nonparametric approach to further elucidate scaling in hyporheic zone processing.

4. Conclusions

We used a conservative tracer, Br^-, and a reactive tracer, Raz, to infer variability in hyporheic zone processing along a first- to fifth-order fluvial network during low and high flow regimes in two consecutive years. Our work provides a standardized approach to comparing hyporheic zone processing along fluvial networks and relates to other studies that have evaluated transient storage across several stream orders (e.g., Briggs et al., 2010; Covino, 2012; Ensign & Doyle, 2006; Gooseff et al., 2013).

The results of this study indicate that hyporheic zone processing throughout the Jemez River is both spatially and temporally dynamic, implying that stream order and seasonal variably in flow influence hyporheic exchange. We found that for our study sites, the parameters related to reactive transport (e.g., mass transfer of reactive tracers and transformation rate coefficients) exhibited more variability than those more closely associated with pure conservative transport (e.g., advection, dispersion, and groundwater input). This implies that the variability in streambed reactivity may be more closely related to *in situ* factors governing reactions such as redox conditions, organic carbon content and nutrient concentrations (Summers et al., 2020), rather than bulk water mass transfer.

We found that the studied portion of the Jemez River fluvial network generally followed the scaling expectations of decreasing hyporheic contributions with discharge based on normalized hyporheic exchange fluxes and reaction rate coefficients. Furthermore, our results demonstrate that while a single summary metric such as the Damköhler number could help us classify overall system behavior (i.e., transport- vs. reaction-limited systems) and scale transport processes across flow regimes, it may also inadvertently mask the behavior of other important scaling relationships. For example, while we observed a trend toward reaction-limited conditions (i.e., decreasing Damköhler number) with increasing discharge, this trend was predominantly driven by a stronger trend of decreasing processing rate coefficients. This, in turn, outweighed the lack of trend with discharge observed for the hyporheic zone residence times (Figure 5).

Our field-based findings suggest that achieving knowledge transferability of hyporheic processing within fluvial networks may be possible, especially when process variability is sampled across multiple stream orders and flow regimes. Therefore, we propose a shift in our traditional approach to investigating scaling patterns in transport processes, which currently relies on the interpretation of studies conducted at multiple sites (mainly in headwater streams) located in different fluvial networks, to a more cohesive, network-centered investigation of processes using the same or readily comparable methods. With this in mind, we call for a more organized collection of reactive transport data within and across fluvial networks to better understand how riverine processing varies over space and time. The inclusion of paired conservative-reactive tracer experiments within multiple fluvial networks would provide evidence to make broader conclusions about how stream order and seasonal flow variations influence hyporheic exchange at the watershed scale. This new emphasis on fluvial network-scale processes will not only improve the predictive ability of existing and new solute transport models but will also generate a more robust understanding of the highly dynamic coupling between human and fluvial systems. Using a stream network approach will thus provide insight into how our highly dynamic interventions and their cumulative effects (e.g., water

uptake, agricultural runoff, and effluent discharges from wastewater treatment plants) impact water quality and the fluvial and terrestrial ecosystems that depend on it.

Acknowledgments
Funding for this work was supported by the following: NSF (HRD-1345169 and CBET-1707042) to R. G. P.; CUAHSI Pathfinder Fellowship and a GSA Grant-in-Aid (RG 1407–16) to K. S. G.; the University of North Carolina at Chapel Hill; the University of New Mexico; the Pueblo of Jemez Department of Natural Resources; and funding through an ETH Zurich Postdoctoral Fellowship to J. K. The authors wish to thank Betsy Summers, James S. Fluke, Fabian Carbajal, Kathryn Beebe, and Justin Nichols for their assistance in the New Mexico fieldwork and lab analyses and Charlotte Hopson, Alexander Smith, Drew Hoag, and Savannah Swinea for their lab analysis assistance in North Carolina. Additional supporting information including Code S1 and the tracer data (Data S1) are available online with the CUAHSI HydroShare program and can be found here: http://www.hydroshare.org/resource/064dbbb2125a483690dfd7d674ba73b6 (Gootman et al., 2020). All data archiving was completed with adherence to the common Enabling FAIR Data Project guidelines.

References

Alexander, R. B., Boyer, E. W., Smith, R. A., Schwarz, G. E., & Moore, R. B. (2007). The role of headwater streams in downstream water quality. *Journal of the American Water Resources Association*, *43*(1), 41–59. https://doi.org/10.1111/j.1752-1688.2007.00005.x

Alexander, R. B., Smith, R. A., & Schwarz, G. E. (2000). Effect of stream channel size on the delivery of nitrogen to the Gulf of Mexico. *Nature*, *403*(6771), 758–761. https://doi.org/10.1038/35001562

Argerich, A., Haggerty, R., Martí, E., Sabater, F., & Zarnetske, J. (2011). Quantification of metabolically active transient storage (MATS) in two reaches with contrasting transient storage and ecosystem respiration. *Journal of Geophysical Research*, *116*, G03034. https://doi.org/10.1029/2010JG001379

Boano, F., Harvey, J. W., Marion, A., Packman, A. I., Revelli, R., Ridolfi, L., & Wörman, A. (2014). Hyporheic flow and transport processes: Mechanisms, models, and biogeochemical implications. *Reviews of Geophysics*, *52*, 603–679. https://doi.org/10.1002/2012RG000417

Boulton, A. J., Findlay, S., Marmonier, P., Stanley, E. H., & Valett, H. M. (1998). The functional significance of the hyporheic zone in streams and rivers. *Annual Review of Ecology and Systematics*, *29*(1), 59–81. https://doi.org/10.1146/annurev.ecolsys.29.1.59

Briggs, M. A., Gooseff, M. N., Peterson, B. J., Morkeski, K., Wollheim, W. M., & Hopkinson, C. S. (2010). Surface and hyporheic transient storage dynamics throughout a coastal stream network. *Water Resources Research*, *46*, W06516. https://doi.org/10.1029/2009WR008222

Brunke, M., & Gonser, T. (1997). The ecological significance of exchange processes between rivers and groundwater. *Freshwater Biology*, *37*, 1–33. https://doi.org/10.1046/j.1365-2427.1997.00143.x

Cibils, A. F., Miller, J. A., Encinias, A. M., Boykin, K. G., & Cooper, B. F. (2008). Monitoring heifer grazing distribution at the Valles Caldera National Preserve. *Rangelands*, *30*(6), 19–23. https://doi.org/10.2111/1551-501X-30.6.19

Coop, J. D., & Givnish, T. J. (2007). Gradient analysis of reversed treelines and grasslands of the Valles Caldera, New Mexico. *Journal of Vegetation Science*, *18*(1), 43–54. https://doi.org/10.1111/j.1654-1103.2007.tb02514.x

Covino, T. P. (2012). The role of stream network nutrient uptake kinetics and groundwater exchange in modifying the timing, magnitude, and form of watershed export, (doctoral dissertation). Retrieved from CiteSeerX. Bozeman, MT: Montana State University.

Craig, SD. (1992). Water resources on the pueblos of Jemez, Zia, and Santa Ana, Sandoval County, New Mexico. Water Resources Investigations Report 89–4091. Denver, Colorado: U.S. Department of the Interior U.S. Geological Survey.

Dallan, E., Regier, P., Marion, A., & González-Pinzón, R. (2020). Does the mass balance of the reactive tracers resazurin and resorufin close at the microbial scale? *Journal of Geophysical Research – Biogeosciences*, *125*, e2019JG005435. https://doi.org/10.1029/2019JG005435

Ensign, S. H., & Doyle, M. W. (2005). In-channel transient storage and associated nutrient retention: Evidence from experimental manipulations. *Limnology and Oceanography*, *50*(6), 1740–1751. https://doi.org/10.4319/lo.2005.50.6.1740

Ensign, S. H., & Doyle, M. W. (2006). Nutrient spiraling in streams and river networks. *Journal of Geophysical Research*, *111*, G04009. https://doi.org/10.1029/2005JG000114

Fetter, C. W. (2001). *Applied hydrogeology*, (4th ed.). Upper Saddle River, N.J: Prentice Hall.

Fischer, H., Kloep, F., Wilzcek, S., & Pusch, M. T. (2005). A river's liver: Microbial processes within the hyporheic zone of a large lowland river. *Biogeochemistry*, *76*(2), 349–371. https://doi.org/10.1007/sl0533-005-6896-y

Freeman, M. C., Pringle, C. M., & Jackson, C. R. (2007). Hydrologic connectivity and the contribution of stream headwaters to ecological integrity at regional scales. *Journal of the American Water Resources Association*, *43*(1), 5–14. https://doi.org/10.1111/j.1752-1688.2007.00002.x

Gelman, A., & Rubin, D. B. (1992). Inference from iterative simulation using multiple sequences. *Statistical Science*, *7*(4), 457–472. https://doi.org/10.1214/ss/1177011136

Gomez-Velez, J. D., & Harvey, J. W. (2014). A hydrogeomorphic river network model predicts where and why hyporheic exchange is important in large basins. *Geophysical Research Letters*, *41*, 6403–6412. https://doi.org/10.1002/2014GL061099

Gomez-Velez, J. D., Harvey, J. W., Cardenas, M. B., & Kiel, B. (2015). Denitrification in the Mississippi River network controlled by flow through river bedforms. *Nature Geoscience*, *8*(October). https://doi.org/10.1038/ngeo2567

González-Pinzón, R., & Haggerty, R. (2013). An efficient method to estimate processing rates in streams. *Water Resources Research*, *49*, 6096–6099. https://doi.org/10.1002/wrcr.20446

González-Pinzón, R., Haggerty, R., & Argerich, A. (2014). Quantifying spatial differences in metabolism in headwater streams. *Freshwater Science*, *33*(3), 798–811. https://doi.org/10.1086/677555

González-Pinzón, R., Haggerty, R., & Myrold, D. D. (2012). Measuring aerobic respiration in stream ecosystems using the resazurin-resorufin system. *Journal of Geophysical Research*, *117*, G00N06. https://doi.org/10.1029/2012JG001965

González-Pinzón, R., Mortensen, J., & Van Horn, D. (2015a). Comment on "solute-specific scaling of inorganic nitrogen and phosphorus uptake in streams" by Hall et al. (2013). *Biogeosciences*, *12*(18), 5365–5369. https://doi.org/10.5194/bg-12-5365-2015

González-Pinzón, R., Ward, A. S., Hatch, C. E., Wlostowski, A. N., Singha, K., Gooseff, M. N., et al. (2015b). A field comparison of multiple techniques to quantify groundwater-surface-water interactions. *Freshwater Science*, *34*(1), 139–160. https://doi.org/10.1086/679738

González-Pinzón, R., Peipoch, M., Haggerty, R., Martí, E., & Fleckenstein, J. H. (2016). Nighttime and daytime respiration in a headwater stream. *Ecohydrology*, *9*(1), 93–100. https://doi.org/10.1002/eco.1615

Gooseff, M. N. (2010). Defining hyporheic zones—Advancing our conceptual and operational definitions of where stream water and groundwater meet. *Geography Compass*, *4*(8), 945–955. https://doi.org/10.1111/j.1749-8198.2010.00364.x

Gooseff, M. N., Bencala, K. E., Scott, D. T., Runkel, R. L., & McKnight, D. M. (2005). Sensitivity analysis of conservative and reactive stream transient storage models applied to field data from multiple-reach experiments. *Advances in Water Resources*, *28*(5), 479–492. https://doi.org/10.1016/j.advwatres.2004.11.012

Gooseff, M. N., Briggs, M. A., Bencala, K. E., McGlynn, B. L., & Scott, D. T. (2013). Do transient storage parameters directly scale in longer, combined stream reaches? Reach length dependence of transient storage interpretations. *Journal of Hydrology*, *483*, 16–25. https://doi.org/10.1016/j.jhydrol.2012.12.046

Gootman, K. S., R. González-Pinzón, Knapp, J. L. A., Garayburu-Caruso, V., & Cable, J. E. (2020). Spatiotemporal variability in transport and reactive processes across a 1st–5th order fluvial network, HydroShare, http://www.hydroshare.org/resource/064dbbb2125a483690dfd7d674ba73b6

Graf, W. L. (2001). Age control: Restoring the physical integrity of America's rivers. *Annals of the Association of American Geographers*, *91*(1), 1–27. https://doi.org/10.1111/0004-5608.00231

Groffman, P. M., Butterbach-Bahl, K., Fulweiler, R. W., Gold, A. J., Morse, J. L., Stander, E. K., et al. (2009). Challenges to incorporating spatially and temporally explicit phenomena (hotspots and hot moments) in denitrification models. *Biogeochemistry*, *93*(1–2), 49–77. https://doi.org/10.1007/s10533-008-9277-5

Haggerty, R. (2002). Power-law residence time distribution in the hyporheic zone of a 2nd-order mountain stream. *Geophysical Research Letters*, *29*(13), 1640. https://doi.org/10.1029/2002GL014743

Haggerty, R., Argerich, A., & Martí, E. (2008). Development of a "smart" tracer for the assessment of microbiological activity and sediment-water interaction in natural waters: The resazurin-resorufin system. *Water Resources Research*, *44*, W00D01. https://doi.org/10.1029/2007WR006670

Haggerty, R., Martí, E., Argerich, A., von Schiller, D., & Grimm, N. B. (2009). Resazurin as a "smart" tracer for quantifying metabolically active transient storage in stream ecosystems. *Journal of Geophysical Research*, *114*, G03014. https://doi.org/10.1029/2008JG000942

Hall, R. O., Baker, M. A., Rosi-Marshall, E. J., Tank, J. L., & Newbold, J. D. (2013). Solute-specific scaling of inorganic nitrogen and phosphorus uptake in streams. *Biogeosciences*, *10*(11), 7323–7331. https://doi.org/10.5194/bg-10-7323-2013

Harvey, C. F., & Gorelick, S. M. (1995). Mapping hydraulic conductivity: Sequential conditioning with measurements of solute arrival time, hydraulic head, and local conductivity. *Water Resources Research*, *31*(7), 1615–1626. https://doi.org/10.1029/95WR00547

Harvey, J., Gomez-Velez, J., Schmadel, N., Scott, D., Boyer, E., Alexander, R., et al. (2019). How hydrologic connectivity regulates water quality in river corridors. *Journal of the American Water Resources Association*, *55*(2), 369–381. https://doi.org/10.1111/1752-1688.1269

Harvey, J. W., Böhlke, J. K., Voytek, M. A., Scott, D., & Tobias, C. R. (2013). Hyporheic zone denitrification: Controls on effective reaction depth and contribution to whole-stream mass balance. *Water Resources Research*, *49*, 6298–6316. https://doi.org/10.1002/wrcr.20492

Harvey, J. W., Drummond, J. D., Martin, R. L., McPhillips, L. E., Packman, A. I., Jerolmack, D. J., et al. (2012). Hydrogeomorphology of the hyporheic zone: Stream solute and fine particle interactions with a dynamic streambed. *Journal of Geophysical Research*, *117*, G00N11. https://doi.org/10.1029/2012JG002043

Harvey, J. W., & Fuller, C. C. (1998). Effect of enhanced manganese oxidation in the hyporheic zone on basin-scale geochemical mass balance. *Water Resources Research*, *34*(4), 623–636. https://doi.org/10.1029/97WR03606

Harvey, J. W., & Gooseff, M. N. (2015). River corridor science: Hydrologic exchange and ecological consequences from bedforms to basins. *Water Resources Research*, *51*, 6893–6922. https://doi.org/10.1002/2015WR017617

Harvey, J. W., Saiers, J. E., & Newlin, J. T. (2005). Solute transport and storage mechanisms in wetlands of the Everglades, South Florida. *Water Resources Research*, *41*, W05009. https://doi.org/10.1029/2004WR003507

Hester, E. T., Cardenas, M. B., Haggerty, R., & Apte, S. V. (2017). The importance and challenge of hyporheic mixing. *Water Resources Research*, *53*, 3565–3575. https://doi.org/10.1002/2016WR020005

Hollenbeck, K. (1998). INVLAP. M: A matlab function for numerical inversion of Laplace transforms by the de Hoog algorithm. Retrieved from https://www.mathworks.com/matlabcentral/answers/uploaded_files/1034/invlap.m

Homer, C. G., Dewitz, J. A., Yang, L., Jin, S., Danielson, P., Xian, G., et al. (2015). Completion of the 2011 National Land Cover Database for the conterminous United States—Representing a decade of land cover change information. *Photogrammetric Engineering and Remote Sensing*, *81*(5), 345–354.

Knapp, J. L. A., & Cirpka, O. A. (2017). Determination of hyporheic travel-time distributions and other parameters from concurrent conservative and reactive tracer tests by local-in-global optimization. *Water Resources Research*, *53*, 4984–5001. https://doi.org/10.1002/2017WR020734

Knapp, J. L. A., & Cirpka, O. A. (2018). A critical assessment of relating resazurin-resorufin experiments to stream metabolism in lowland streams. *Journal of Geophysical Research – Biogeosciences*, *123*, 3583–3555. https://doi.org/10.1029/2018JG004797

Knapp, J. L. A., González-Pinzón, R., Drummond, J. D., Larsen, L. G., Cirpka, O. A., & Harvey, J. W. (2017). Tracer-based characterization of hyporheic exchange and benthic biolayers in streams. *Water Resources Research*, *53*, 1575–1594. https://doi.org/10.1002/2016WR019393

Knapp, J. L. A., González-Pinzón, R., & Haggerty, R. (2018). The resazurin-resorufin system: Insights from a decade of "smart" tracer development for hydrologic applications. *Water Resources Research*, *54*, 6877–6889. https://doi.org/10.1029/2018WR023103

Krause, S., Hannah, D. M., Fleckenstein, J. H., Heppell, C. M., Kaeser, D., Pickup, R., et al. (2011). Inter-disciplinary perspectives on processes in the hyporheic zone. *Ecohydrology*, *4*(4), 481–499. https://doi.org/10.1002/eco

Krause, S., Lewandowski, J., Grimm, N. B., Hannah, D. M., Pinay, G., McDonald, K., et al. (2017). Ecohydrological interfaces as hot spots of ecosystem processes. *Water Resources Research*, *53*, 6359–6376. https://doi.org/10.1002/2016WR019516

Lemke, D., González-Pinzón, R., Liao, Z., Wöhling, T., Osenbrück, K., Haggerty, R., & Cirpka, O. A. (2014). Sorption and transformation of the reactive tracers resazurin and resorufin in natural river sediments. *Hydrology and Earth System Sciences*, *18*(8), 3151–3163. https://doi.org/10.5194/hess-18-3151-2014

Lemke, D., Liao, Z., Wöhling, T., Osenbrück, K., & Cirpka, O. A. (2013). Concurrent conservative and reactive tracer tests in a stream undergoing hyporheic exchange. *Water Resources Research*, *49*, 3024–3037. https://doi.org/10.1002/wrcr.20277

Liao, Z., & Cirpka, O. A. (2011). Shape-free inference of hyporheic travel time distributions from synthetic conservative and "smart" tracer tests in streams. *Water Resources Research*, *47*, W07510. https://doi.org/10.1029/2010WR009927

Magliozzi, C., Grabowski, R., Packman, A. I., & Krause, S. (2018). Toward a conceptual framework of hyporheic exchange across spatial scales. *Hydrology and Earth System Sciences*, *22*, 6163–6185. https://doi.org/10.5194/hess-2018-268

McClain, M. E., Boyer, E. W., Dent, C. L., Gergel, S. E., Grimm, N. B., Groffman, P. M., et al. (2003). Biogeochemical hot spots and hot moments at the interface of terrestrial and aquatic ecosystems. *Ecosystems*, *6*(4), 301–312. https://doi.org/10.1007/s10021-003-0161-9

McGibbon, C., Crossey, L. J., Karlstrom, K. E., & Grulke, T. (2018). Carbonic springs as distal manifestations of geothermal systems, highlighting the importance of fault pathways and hydrochemical mixing: Example from the Jemez Mountains, New Mexico. *Applied Geochemistry*, 45–247. https://doi.org/10.1016/j.apgeochem.2018.08.015

McIntosh, J. C., Schaumberg, C., Perdrial, J., Harpold, A., Vázquez-Ortega, A., Rasmussen, C., et al. (2017). Geochemical evolution of the critical zone across variable time scales informs concentration-discharge relationships: Jemez River basin critical zone observatory. *Water Resources Research*, *53*, 4169–4196. https://doi.org/10.1002/2016WR019712

New Mexico Climate Center. Cooperative Observer Program Stations. (2018) Jul [accessed 2018 Jul]. https://weather.nmsu.edu/coop/

Nowinski, J. D., Cardenas, M. B., & Lightbody, A. F. (2011). Evolution of hydraulic conductivity in the floodplain of a meandering river due to hyporheic transport of fine materials. *Geophysical Research Letters*, *38*, L01401. https://doi.org/10.1029/2010GL045819

Ocampo, C. J., Oldham, C. E., & Sivapalan, M. (2006). Nitrate attenuation in agricultural catchments: Shifting balances between transport and reaction. *Water Resources Research*, *42*, W01408. https://doi.org/10.1029/2004WR003773

Oldham, C. E., Farrow, D. E., & Peiffer, S. (2013). A generalized Damköhler number for classifying material processing in hydrological systems. *Hydrology and Earth System Sciences*, *17*(3), 1133–1148. https://doi.org/10.5194/hess-17-1133-2013

Orghidan, T. (1959). A new habitat of subsurface waters: The hyporheic biotope. *Fundamental and Applied Limnology/Archiv Für Hydrobiologie*, *176*(4), 291–302. https://doi.org/10.1127/1863-9135/2010/0176-0291

Patil, S., Covino, T. P., Packman, A. I., McGlynn, B. L., Drummond, J. D., Payn, R. A., & Schumer, R. (2013). Intrastream variability in solute transport: Hydrologic and geomorphic controls on solute retention. *Journal of Geophysical Research - Earth Surface*, *118*, 413–422. https://doi.org/10.1029/2012JF002455

Payn, R. A., Gooseff, M. N., Benson, D. A., Cirpka, O. A., Zarnetske, J. P., Bowden, W. B., ... Bradford, J. H. (2008). Comparison of instantaneous and constant-rate stream tracer experiments through non-parametric analysis of residence time distributions. *Water Resources Research*, *44*(6). https://doi.org/10.1029/2007WR006274

Pinay, G., Peiffer, S., De Dreuzy, J. R., Krause, S., Hannah, D. M., Fleckenstein, J. H., et al. (2015). Upscaling nitrogen removal capacity from local hotspots to low stream orders' drainage basins. *Ecosystems*, *18*(6), 1101–1120. https://doi.org/10.1007/s10021-015-9878-5

Ren, J., & Packman, A. I. (2007). Changes in fine sediment size distributions due to interactions with streambed sediments. *Sedimentary Geology*, *202*(3), 529–537. https://doi.org/10.1016/j.sedgeo.2007.03.021

Runkel, R. L. (1998). One-dimensional transport with inflow and storage (OTIS): A solute transport model for streams and rivers. Water-Resources Investigations Report 98-4018, 1–80. https://doi.org/10.3133/wri984018

Small, E. E., & McConnell, J. R. (2008). Comparison of soil moisture and meteorological controls on pine and spruce transpiration. *Ecohydrology*, *1*, 205–214. https://doi.org/10.1002/eco

Smith, R. L., Bailey, R. A., & Ross, C. S. (1970). *Geologic map of the Jemez Mountains, New Mexico*, *Miscellaneous Geologic Investigations Map I-571*, (). Reston, VA, US: USGS.

Stonedahl, S. H., Harvey, J. W., & Packman, A. I. (2013). Interactions between hyporheic flow produced by stream meanders, bars, and dunes. *Water Resources Research*, *49*, 5450–5461. https://doi.org/10.1002/wrcr.20400

Strahler, A. N. (1952). Hypsometric (area-altitude) analysis of erosional topography. *Geological Society of America Bulletin*, *63*(11), 1117–1142. https://doi.org/10.1130/0016-7606(1952)63

Stream Solute Workshop (1990). Concepts and methods for assessing solute dynamics in stream ecosystems. *Journal of the North American Benthological Society*, *9*(2), 95–119.

Summers, B. M., Van Horn, D. J., González-Pinzón, R., Bixby, R. J., Grace, M. R., Sherson, L. R., et al. (2020). Long-term data reveal highly-variable metabolism and transitions in trophic status in a montane stream. *Freshwater Science*. https://doi.org/10.1086/708659

Tank, J. L., Rosi-Marshall, E. J., Baker, M. A., & Hall, R. O. Jr. (2008). Are rivers just big streams? A pulse method to quantify nitrogen demand in a large river. *Ecology*, *89*(10), 2935–2945. https://doi.org/10.1890/07-1315.1

Terzi, R.A. (1981). Hydrometric field manual—Measurement of streamflow, Environment Canada, Inland Waters Directorate, Water Resources Branch, 1981.

United States Geological Survey (2018). National Water Information Systems. Site Map for New Mexico. 7/18 [accessed 7/18]. https://waterdata.usgs.gov/nm/nwis/nwismap/?site_no=08328950andagency_cd=USGS

Vomocil, J. A. (1965). Porosity. In C. A. Black (Ed.), *Methods of soil analysis*, (pp. 299–314). Madison, Wisconsin: American Society of Agronomy.

Vrugt, J. A., ter Braak, C. J. F., Diks, C. G. H., Robinson, B. A., Hyman, J. M., & Higdon, D. (2009). Accelerating Markov chain Monte Carlo simulation by differential evolution with self-adaptive randomized subspace sampling. *International Journal of Nonlinear Sciences and Numerical Simulation*, *10*(3), 273–290. https://doi.org/10.1515/IJNSNS.2009.10.3.273

Wagner, B. J., & Harvey, J. W. (1997). Experimental design for estimating parameters of rate-limited mass transfer: Analysis of stream tracer studies. *Water Resources Research*, *33*(7), 1731. https://doi.org/10.1029/97WR01067

Ward, A. S. (2016). The evolution and state of interdisciplinary hyporheic research. *Wiley Interdisciplinary Reviews Water*, *3*, 83–103. https://doi.org/10.1002/wat2.1120

Ward, A. S., Payn, R. A., Gooseff, M. N., McGlynn, B. L., Bencala, K. E., Kelleher, C. A., et al. (2013). Variations in surface water-ground water interactions along a headwater mountain stream: Comparisons between transient storage and water balance analyses. *Water Resources Research*, *49*, 3359–3374. https://doi.org/10.1002/wrcr.20148

Ward, A. S., Wondzell, S. M., Schmadel, N. M., Herzog, S., Zarnetske, J. P., Baranov, V., et al. (2019). Spatial and temporal variation in river corridor exchange across a 5th order mountain stream network. *Hydrology and Earth Systems Sciences Discussion*, *23*(12), 5199–5225. https://doi.org/10.5194/hess-2019-108

White, A. F., Chuma, N. J., & Goff, F. (1992). Mass transfer constraints on the chemical evolution of an active hydrothermal system, Valles caldera, New Mexico. *Journal of Volcanology and Geothermal Research*, *49*, 233–253. https://doi.org/10.1016/0377-0273(92)90016-7

Woessner, W. W. (2000). Stream and fluvial plain ground water interactions: Rescaling hydrogeologic thought. *Ground Water*, *38*(3), 423–429. https://doi.org/10.1111/j.1745-6584.2000.tb00228.x

Wohl, E. (2015). Legacy effects on sediments in river corridors. *Earth-Science Reviews*, *147*, 30–53. https://doi.org/10.1016/j.earscirev.2015.05.001

Wondzell, S. M. (2011). The role of the hyporheic zone across stream networks. *Hydrological Processes*, *25*(22), 3525–3532. https://doi.org/10.1002/hyp.8119

Wroblicky, G. J., Campana, M. E., Valett, H. M., & Dahm, N. (1998). Seasonal variation in surface-subsurface water exchange and lateral hyporheic area of two stream-aquifer systems. *Water Resources Research*, *34*(3), 317–328. https://doi.org/10.1029/97WR03285

Xie, X., & Zhang, D. (2010). Data assimilation for distributed hydrological catchment modeling via ensemble Kalman filter. *Advances in Water Resources*, *33*(6), 678–690. https://doi.org/10.1016/j.advwatres.2010.03.012

References From the Supporting Information

Kasahara, T., & Wondzell, S. M. (2003). Geomorphic controls on hyporheic exchange flow in mountain streams. *Water Resources Research*, *39*(1), 1005. https://doi.org/10.1029/2002WR001386

Laloy, E., & Vrugt, J. A. (2012). High-dimensional posterior exploration of hydrologic models using multiple-try DREAM (ZS) and high-performance computing. *Water Resources Research*, *48*, W01526. https://doi.org/10.1029/2011WR010608

Vrugt, J. A. (2016). Markov chain Monte Carlo simulation using the DREAM software package: Theory, concepts, and MATLAB implementation. *Environmental Modelling and Software*, *75*, 273–316. https://doi.org/10.1016/j.envsoft.2015.08.013

Vrugt, J. A., ter Braak, C. J. F., Clark, M. P., Hyman, J. M., & Robinson, B. A. (2008). Treatment of input uncertainty in hydrologic modeling: Doing hydrology backward with Markov chain Monte Carlo simulation. *Water Resources Research*, *44*, W00B09. https://doi.org/10.1029/2007WR006720

Wondzell, S. M. (2006). Effect of morphology and discharge on hyporheic exchange flows in two small streams in the Cascade Mountains of Oregon, USA. *Hydrological Processes*, *20*(2), 267–287. https://doi.org/10.1002/hyp.5902

Wondzell, S. M., & Swanson, F. J. (1996). Seasonal and storm dynamics of the hyporheic zone of a 4th-order mountain stream I. Hydrologic processes. *Journal of the North American Benthological Society*, *15*(1), 3–19. https://doi.org/10.2307/1467429